Generation and tomography of arbitrary optical qubits using transient collective atomic excitations

T. Brannan,[1] Z. Qin,[1,2] A. MacRae,[1,3] and A. I. Lvovsky[1,4,*]

[1]*Institute for Quantum Science and Technology, University of Calgary, Calgary, Alberta T2N 1N4, Canada*

[2]*Quantum Institute for Light and Atoms, State Key Laboratory of Precision Spectroscopy, East China Normal University, Shanghai 200062, China*

[3]*Department of Physics, University of California, Berkeley, California 94720, USA*

[4]*Russian Quantum Center, 100 Novaya St., Skolkovo, Moscow 143025, Russia*

**Corresponding author: lvov@ucalgary.ca*

Received June 25, 2014; accepted August 2, 2014;
posted August 11, 2014 (Doc. ID 214612); published September 15, 2014

We demonstrate the preparation of heralded Fock-basis qubits ($a|0\rangle + b|1\rangle$) from transient collective spin excitations in a hot atomic vapor. The preparation event is heralded by Raman-scattered photons in a four-wave mixing process seeded by a weak coherent optical excitation. The amplitude and phase of the seed field allow arbitrary control over the qubit coefficients. The qubit state is characterized using balanced homodyne tomography. © 2014 Optical Society of America

OCIS codes: (270.0270) Quantum optics; (270.5585) Quantum information and processing.
http://dx.doi.org/10.1364/OL.39.005447

Quantum state engineering remains a central challenge for the development of quantum technologies. There has been a great deal of progress in preparing and measuring interesting quantum states in the optical domain, driven by the attractiveness of light as a mediator for quantum information and quantum communication [1]. Quantum state engineering has also been demonstrated in many other quantum systems [2], including superconducting circuits [3] and trapped ion ensembles [4].

While the primary workhorse of quantum-optical state engineering has so far been parametric downconversion, recent advancements in quantum light–atom interfacing allows for similar accomplishments using a very different physical phenomenon: four-wave mixing in atomic ensembles. In this Letter, we present a basic example of such engineering: preparation of a single-rail optical qubit. This result is significant in particular because our approach allows extension of quantum-state engineering to a new domain of collective spin excitations (CSEs) in atomic ensembles. This would prove valuable, as atomic systems have shown to be a promising candidate for interfacing quantum information between light and matter [5]. Engineering arbitrary quantum states of these atomic CSEs can find applications in quantum memories [6], quantum repeaters [7], quantum logic gates [8], and quantum metrology [9].

Our system employs coherent double Raman scattering (four-wave mixing) in an ensemble of three-level Λ-type atoms (Fig. 1(b)], akin to the DLCZ protocol [7]. If all atoms are initially in one ground state $|b\rangle$, emission of a single Raman-scattered photon corresponds to a "write" event where one atom has transitioned to the other ground state $|c\rangle$. Because the atoms are indistinguishable, the excitation occurs collectively over all the atoms within the interaction region, leaving the atomic ensemble in the single-quantum CSE state

$$|1\rangle = \frac{1}{\sqrt{N}} \sum_{n=1}^{N} e^{i\phi_n} |b_1 \ldots b_{n-1} c_n b_{n+1} \ldots b_N\rangle. \tag{1}$$

Here, N is the total number of interacting atoms, and ϕ_n gives the phase associated with the recoil of each atom. The Hamiltonian for the Raman scattering is

$$\hat{H} = \gamma(\hat{a}_i \hat{a}_{\mathrm{CSE}} + \hat{a}_i^\dagger \hat{a}_{\mathrm{CSE}}^\dagger), \tag{2}$$

where $\hat{a}_i$ and $\hat{a}_{\mathrm{CSE}}$ are the annihilation operators for the scattered photon (which we call "idler") and the atomic CSE, respectively, and γ is the coupling constant.

Subsequent excitation of the $|c\rangle \to |a\rangle$ transition returns the atom to the original state $|b\rangle$, and the CSE is transformed into an optical state coherently emitted along the $|a\rangle \to |b\rangle$ transition. Constructive interference for this read transition occurs when phase-matching conditions are met, collectively enhancing the emission into a specific "signal" mode [7], which can be measured using homodyne tomography.

In our experiment, single, strong continuous laser pumps both of the read and write transitions are involved in DLCZ simultaneously. The read and write transitions, with the associated emission of signal and idler photons,

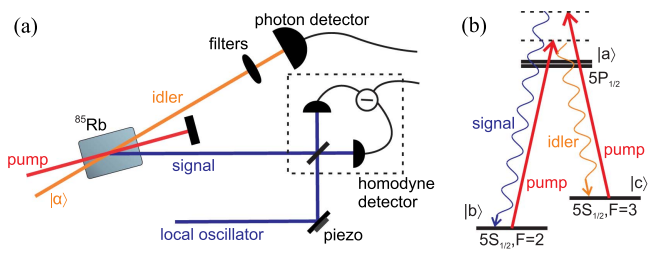

Fig. 1. (a) Experimental setup. Weak seed beam $|\alpha\rangle$ is introduced into the cell along the same mode as the four-wave mixing idler and subsequently filtered and detected. Due to the identical spatial mode and high time resolution of the single-photon counting module, the source of the detection events is fundamentally indistinguishable, which projects the signal onto a controllable superposition state. (b) Three-level lambda system in ^{85}Rb; a strong pump drives both Raman transitions, resulting in emission of photon pairs into the signal and idler channels.

 © 2014 Optical Society of America

occur at the same time so the CSE is of transient character [10]. In this case, Hamiltonian (2) takes the form analogous to that of spontaneous parametric downconversion

$$\hat{H} = \gamma(\hat{a}_i\hat{a}_s + \hat{a}_i^\dagger\hat{a}_s^\dagger), \tag{3}$$

where s and i refer to the signal and idler modes. We use this interaction for quantum state engineering of the signal optical mode. In future experiments, the read and write events can be separated in time by switching to pulsed excitations [11], allowing for preparation of atomic states by the same technique.

We experimentally generate arbitrary Fock-basis qubits, following the method reminiscent of Bimbard *et al.* [12]. We seed the idler channel with (2) a weak coherent state $|\alpha\rangle$. Assuming that the initial signal state is vacuum (all atoms in $|b\rangle$), interaction under Hamiltonian (3) for time t leads, in the first order in α and γ, to the following state

$$|\Psi_{\text{out}}\rangle = |0_i, 0_s\rangle + \alpha|1_i, 0_s\rangle - i\frac{\gamma t}{\hbar}|1_i, 1_s\rangle. \tag{4}$$

In writing Eq. (4), we used $|\alpha\rangle \approx |0\rangle + \alpha|1\rangle$ and $e^{-i\hat{H}t/\hbar} \approx \hat{I} - i\hat{H}t/\hbar$. Now, if we perform photon detection in the idler mode, a single detection event will occur with probability

$$\text{pr}_{\text{count}} = |\alpha|^2 + (|\gamma|t/\hbar)^2 \tag{5}$$

projecting the signal mode onto

$$|\psi_s\rangle = \alpha|0\rangle - i\frac{\gamma t}{\hbar}|1\rangle. \tag{6}$$

In other words, because the photon detector cannot distinguish between a click coming from the coherent beam or from Raman scattering, the state of the signal collapses into a superposition corresponding to the situations where Raman scattering has and has not occurred. The relative amplitudes of the vacuum and single-photon terms in Eq. (6) can be controlled by the amplitude of the weak coherent beam, whereas their relative phase is determined by the optical phase shift between that beam and the pump. In this way, any arbitrary single-rail optical qubit can be created.

Our Λ system employs the 795 nm D1 multiplet in ^{85}Rb, which is shown in Fig. 1(b). Both optical transitions are driven by a single laser, which is blue-detuned by 0.8 GHz from the $|5S_{1/2}, F = 2\rangle \to |5P_{1/2}\rangle$ ($|b\rangle \to |a\rangle$) transition and by 3.9 GHz from the $|5S_{1/2}, F = 3\rangle \to |5P_{1/2}\rangle$ ($|c\rangle \to |a\rangle$) transition. This detuning is chosen to avoid absorption losses while retaining reasonable nonlinearity.

The experimental setup is shown in Fig. 1(a). The 1 W pump beam at 795 nm is generated by a Tekhnoscan TIS-SF 777 Ti:Sapphire laser and passes through a ^{85}Rb gas cell heated to 107°C. In the absence of the coherent seed beam, a quantum four-wave mixing process leads to the generation of correlated signal and idler photons along phase-matched directions [13]. A weak coherent beam $|\alpha\rangle$ is generated at the same frequency as the idler photons by double-passing a small part of the master laser field through a 1.54 GHz acousto-optical modulator. This beam is attenuated, using a series of neutral-density filters, wave plates, and polarizing beam splitters, to the single-photon level. It is then passed through the cell in a spatial mode consistent with that of the idler photons from the four-wave mixing. Subsequently, this mode is spectrally filtered using a 55 MHz linewidth monolithic filter cavity [14] and spatially filtered using a single-mode fiber before being measured with a single-photon detector.

Heralded by a click in the photon detector, we measure the state of the signal using a homodyne detector with a 100 MHz bandwidth [15]. The local oscillator is provided by a 20 mW diode laser phase-stabilized with respect to the pump using an optical phase-lock loop [16]. The homodyne detector photocurrent is integrated over a temporal mode that is determined from the signal variance as a function of time [10] to give a single quadrature value for each click event.

Remarkably, this technique automatically ensures indistinguishability between photons from the coherent state and the atomic source. This indistinguishability is not inherent: while the Raman scattering is broadband, the bandwidth of the coherent state is determined by that of the master laser—i.e., is of the order of a few kHz. However, precision timing of the photon detection events (on a scale of hundreds of picoseconds) combined with spectral filtering with a width of 55 MHz projects all photons onto indistinguishable transform-limited wave packets, with the spectrum determined by the transmissivity of the spectral filter and the timing determined by the detection event [17].

A piezoelectric transducer in the local oscillator path permits phase variation as required for homodyne tomography. After 100,000 quadrature values are collected, the quantum state of the signal is reconstructed using an iterative maximum-likelihood algorithm [18,19].

We reconstruct the density matrix of the signal state that is generated for a range of coherent state amplitudes $|\alpha|$. Figure 2 shows a comparison between a single-photon Fock state ($\alpha = 0$) and a sample qubit ($\alpha\hbar/\gamma t = 0.56$). In the latter case, the off-diagonal element ρ_{01} of the density matrix arises, demonstrating that the two components of the qubit are in a coherent superposition.

Figures 3(a) and 3(b) plot elements ρ_{11} and ρ_{01} of the reconstructed density matrix as a function of the added count rate in the idler channel due to the seed beam. The added count rate is comparable to the count rate of 335 kHz observed at $\alpha = 0$. The blue circles show experimentally measured data points, with the error bars given by the standard deviation from multiple measurements. The dashed red curves show theoretical predictions obtained given by Eqs. (5) and (6), subjected to linear losses along the signal channel. The solid black curves follow a similar model but take into account higher photon number components and the imperfect detector efficiency in the idler channel. Limited homodyne detector bandwidth leads to a mismatch between the measured temporal mode and that of the qubit, which has the same effect as spatial mode mismatch and optical losses [17,20]. All the sources of loss contribute to a combined signal

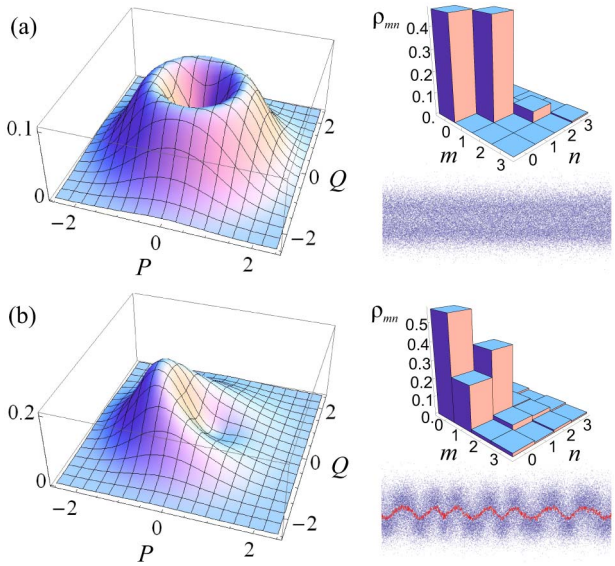

Fig. 2. Reconstructed quantum states. (a) Single-photon Fock state obtained in the absence of the seed ($\alpha = 0$). Density matrix has $\rho_{11} = 0.47$, with a corresponding dip in the Wigner function at the origin and no phase dependence in the quadrature data. (b) Reconstructed state for a generated qubit in the case where 24% of the photon detection events are coming from $|\alpha\rangle$. Off-diagonal elements of the density matrix and phase dependence in the quadrature data indicate coherence, leading to a displacement of the peak of the Wigner function from the origin. Despite the significantly increased vacuum component, the off-diagonal terms contribute to a generalized efficiency of 46%.

channel loss of 51%. Other best-fit parameters include a combined loss of 90% in the idler channel and the pair production amplitude, which corresponds to $\gamma t/\hbar = 0.22$. The best-fit loss parameters are consistent with those measured directly, and the pair production amplitude is consistent with the magnitude of the two-photon component of the generated state [10].

All the qubit states observed in our experiment are nonclassical according to the Mandel criterion $Q = (\langle \Delta n^2 \rangle - \langle n \rangle)/\langle n \rangle < 0$, where n refers to the observable photon number [21]. The experimentally determined value of the Mandel parameter ranges from −0.10 to −0.37. The quality of the generated qubits can also be estimated from the experimental data by using the generalized efficiency [22,23], defined as the lowest possible value of T such that the state observed experimentally can be obtained from another state by transmitting through a loss channel with transmissivity T. Neglecting the photon number terms above 1, the generalized efficiency is given by

$$\mathcal{E}(\hat{\rho}) = \frac{\rho_{11}}{1 - |\rho_{01}|^2/\rho_{11}}. \tag{7}$$

This quantity is displayed in Fig. 3(c). Ideally, the generalized efficiency is expected to be independent of α. However, imperfect photon detectors and the presence of higher photon number components introduce a small dependence on α in the generalized efficiency. The efficiency can be improved, for example, by using a narrower spectral filter for the idler photons that would make the heralded signal photons longer, thereby

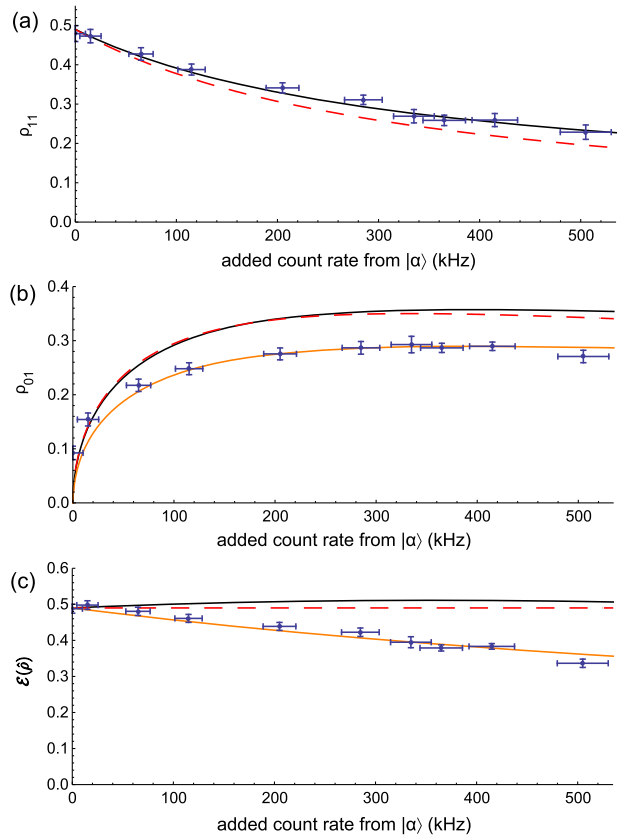

Fig. 3. Experimental results. Density matrix elements (a) ρ_{11} and (b) ρ_{01} are shown, each as a function of the added count rate in the idler channel corresponding to increasing intensity of the seed coherent state. (c) Generalized efficiency $\mathcal{E}(\hat{\rho})$ is calculated over the same range of $|\alpha|$. Solid black lines are generated using a theoretical model of the four-wave mixing process considering photon number terms up to four, taking into account imperfect detection efficiency and losses in both the signal and idler channels. Dashed red curves use the simplified model given by Eq. (6) with the losses only in the signal. Orange curves consider a reduction of ρ_{01} by a constant factor of 0.81 with respect to the black lines.

reducing the effects of the finite homodyne detection bandwith.

From Fig. 3, the theoretical model (black) predicts the experimental behavior for ρ_{11} very well; however, the experimental data for ρ_{01} are below the model by what appears to be a constant factor. This indicates that there is some decoherence between the $|0\rangle$ and $|1\rangle$ components of the qubit. The orange curves in Fig. 3 show the fit with ρ_{01} decreased by a factor of 0.81. The source of this decoherence could not be determined; however, the thermal background contamination was measured to be too weak to cause this effect. This decoherence could come from some residual distinguishability between the seed beam photons and photons from four-wave mixing events or uncertainties when reconstructing the qubit phase for each measurement event.

In summary, we have shown experimental creation and measurement of an arbitrary Fock-state qubit using four-wave mixing seeded by a weak coherent state. This scheme can be advanced to state engineering in a long-lived CSE with delayed, on-demand readout, akin

to a recent experiment [11]. The entanglement emerging thanks to Hamiltonian (2) enables preparation of quantum states of the CSE by performing measurements on the idler mode. While in "classic" DLCZ, detection of the idler photon heralds the creation of a single-quantum CSE, more sophisticated measurements, such as those presented in this Letter, permit engineering of more complex, potentially arbitrary, atomic states. Subsequent excitation of the $|c\rangle \rightarrow |a\rangle$ transition allows for "reading out" the prepared state, converting it to optical form and permitting its characterization using homodyne tomography. Progress along these lines would have significant applicability for quantum light sources, quantum memories, and quantum repeaters.

We thank C. Simon and J. Jing for their helpful suggestions. This project is supported by NSERC and CIFAR. The fourth author is a CIFAR Fellow. The second author is supported by the China Scholarship Council.

References

1. A. I. Lvovsky and M. Raymer, Rev. Mod. Phys. **81**, 299 (2009).
2. R. Blatt, G. J. Milburn, and A. I. Lvovsky, J. Phys. B **46**, 100201 (2013).
3. M. Hofheinz, H. Wang, M. Ansmann, R. Bialczak, E. Lucero, M. Neeley, A. O'Connell, D. Sank, J. Wenner, J. Martinis, and A. Cleland, Nature **459**, 546 (2009).
4. D. Leibfried, E. Knill, S. Seidelin, J. Britton, R. B. Blakestad, J. Chiaverini, D. B. Hume, W. M. Itano, J. D. Jost, C. Langer, R. Ozeri, R. Reichle, and D. J. Wineland, Nature **438**, 639 (2005).
5. K. Hammerer, A. S. Sørensen, and E. S. Polzik, Rev. Mod. Phys. **82**, 1041 (2010).
6. A. I. Lvovsky, W. Tittel, and B. C. Sanders, Nat. Photonics **3**, 706 (2009).
7. L. M. Duan, M. D. Lukin, J. I. Cirac, and P. Zoller, Nature **414**, 413 (2001).
8. L. You and M. S. Chapman, Phys. Rev. A **62**, 052302 (2000).
9. S.-W. Chiow, T. Kovachy, H.-C. Chien, and M. A. Kasevich, Phys. Rev. Lett. **107**, 130403 (2011).
10. A. MacRae, T. Brannan, R. Achal, and A. I. Lvovsky, Phys. Rev. Lett. **109**, 033601 (2012).
11. E. Bimbard, R. Boddeda, N. Vitrant, A. Grankin, V. Parigi, J. Stanojevic, A. Ourjoumtsev, and P. Grangier, Phys. Rev. Lett. **112**, 033601 (2014).
12. E. Bimbard, N. Jain, A. MacRae, and A. I. Lvovsky, Nat. Photonics **4**, 243 (2010).
13. V. Boyer, A. Marino, R. Pooser, and P. Lett, Science **321**, 544 (2008).
14. P. Palittapongarnpim, A. MacRae, and A. I. Lvovsky, Rev. Sci. Instrum. **83**, 066101 (2012).
15. R. Kumar, E. Barrios, A. MacRae, E. Cairns, E. H. Huntington, and A. I. Lvovsky, Opt. Commun. **285**, 5259 (2012).
16. J. Appel, A. MacRae, and A. I. Lvovsky, Meas. Sci. Technol. **20**, 055302 (2009).
17. T. Aichele, A. I. Lvovsky, and S. Schiller, Eur. Phys. J. D **18**, 237 (2002).
18. A. I. Lvovsky, J. Opt. B **6**, S556 (2004).
19. J. Řeháček, Z. Hradil, E. Knill, and A. I. Lvovsky, Phys. Rev. A **75**, 042108 (2007).
20. J. Appel, D. Hoffman, E. Figueroa, and A. I. Lvovsky, Phys. Rev. A **75**, 035802 (2007).
21. L. Mandel, Opt. Lett. **4**, 205 (1979).
22. D. W. Berry, A. I. Lvovsky, and B. C. Sanders, Opt. Lett. **31**, 107 (2006).
23. D. W. Berry and A. I. Lvovsky, Phys. Rev. Lett. **105**, 203601 (2010).